Silicon–Rich Bainitic Steel Welds†

H. K. D. H. Bhadeshia*, M. Lord** and L. –E. Svensson***

Abstract

Ordinary bainite consists of a mixture of plates of ferrite and cementite particles. The cementite precipitates from carbon–enriched austenite, a reaction which can be suppressed by alloying the steel with silicon. The austenite then becomes stabilised by the carbon and the resulting microstructure can be tough and strong. This phenomenon has been exploited in the design of bainitic steels but never in the context of welding alloys. We report here an investigation of the properties of low–alloy steel welding alloys containing deliberate and relatively large concentrations of silicon, and propose a mechanism for the influence of silicon on the stability of cementite.

KEY WORDS: (Silicon) (Weld Metal) (Cementite) (Bainite) (Paraequilibrium)

1. Introduction

Silicon inhibits the precipitation of cementite. Concentrations of about 2wt% silicon can change a brittle, cementite–rich white cast–iron into a ductile graphite–rich grey cast–iron. In high–strength steels the silicon is used to control the tempering of martensite [1–6]. Indeed, this is the basis of the successful very strong steel, $300M$, containing about 1.6 wt.% Si; in this case the rate at which cementite precipitates from supersaturated martensite is reduced when compared with a corresponding steel without the silicon [7].

Silicon also retards the precipitation of cementite from austenite [8–16]. There is a new class of high–strength steels which exploit this principle. By adding sufficient silicon, it is possible to produce a distinctive microstructure, consisting of a mixture of bainitic ferrite, carbon–enriched retained austenite and some martensite [17]. In the past, the full benefits of this carbide–free bainitic microstructure have not been realised. This is because the bainite reaction stops well before equilibrium is reached, *i.e.* when the carbon concentration of the residual austenite reaches a point given by the T_0 curve, beyond which diffusionless growth is prevented. The T_0 curve is the locus of points on a plot of temperature versus carbon concentration, where the free energies of austenite and ferrite of the same chemical composition are identical. Because the bainite reaction is limited by the T_0 curve rather than when equilibrium is achieved, large regions of austenite remain in the final microstructure. These can under stress decompose into hard and potentially brittle martensite [17].

Bhadeshia & Edmonds [18] first presented the design procedure which avoids this difficulty in three ways: by adjusting the T_0 curve using substitutional solutes; by controlling the mean carbon concentration; and by minimising the transformation temperature. Steels were designed on this basis and when tested, revealed a reduction in the ductile–brittle transition temperature of more than 100 K [19].

Fracture toughness measurements confirmed the remarkable levels of toughness that could be achieved, in some cases matching the expensive marageing steels [20]. Other aspects of the theory have been verified using a variety of advanced research techniques, reviewed in [17].

The first major commercial exploitation came with the development of a kinetic theory [17] to complement the thermodynamics inherent in the T_0 concept, so that continuous cooling transformation which is typical in industry, could be dealt with. This led to the invention and manufacture of a bainitic steel with outstanding wear and rolling–contact fatigue resistance. The steel transforms into the correct microstructure during the routine manufacturing process used for making rails [21].

† Received on January 31, 2003
* Professor, University of Cambridge, UK
** Graduate Student, University of Cambridge, UK
*** Senior Metallurgist, Volvo Trucks, Sweden

Transactions of JWRI is published by Joining and Welding Research Institute of Osaka University, Ibaraki, Osaka 567-0047, Japan

Some further achievements of the design procedure [18] are illustrated in Fig. 1a, including our most recent research [22,23] in which gun barrel bainitic steels with the highest strength/toughness combinations ever recorded were designed theoretically and verified experimentally. Toughness values of nearly 130 MPa $m^{\frac{1}{2}}$ have been obtained for strength in the range 1600–1700 MPa (Fig. 1a). Current work is dealing with steels with a strength of 2500 MPa and a toughness in excess of 30 MPa $m^{\frac{1}{2}}$ [24].

The purpose of the present work was to see whether the principles used in the design of wrought bainitic steels can be applied to produce high–strength welding alloys. A study of welding alloys containing relatively large concentrations of silicon was by conducted by Evans [25] but the alloys all were of a low hardenability and hence had conventional microstructures of allotriomorphic ferrite, Widmanstätten ferrite, acicular ferrite and microphases.

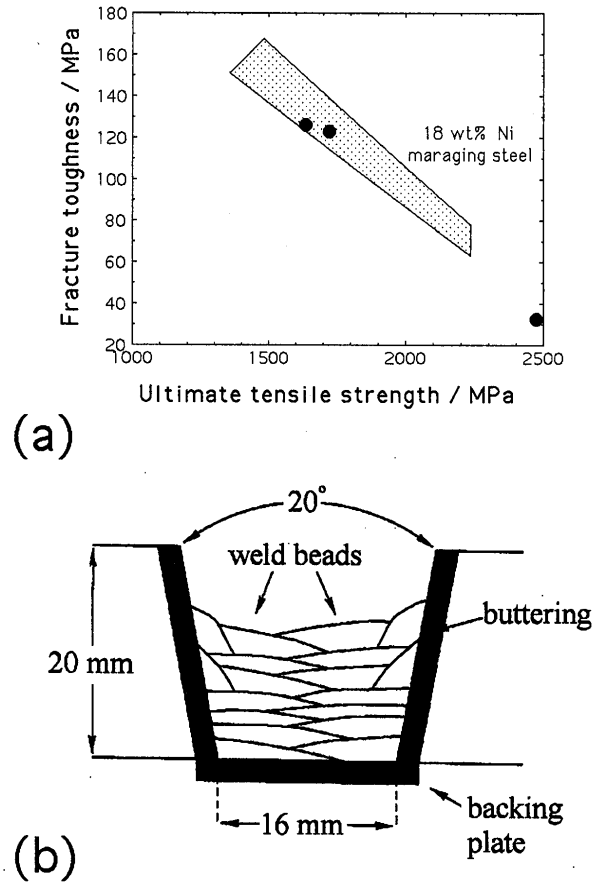

Fig. 1: (a) Properties of mixed microstructures of bainitic ferrite and austenite (points), versus those of expensive marageing steels [25]. (b) Weld preparation.

2. Experimental Method

The experimental welds were fabricated using the manual metal arc welding process and 4 mm diameter electrodes, at the ESAB AB laboratories in Sweden. The study was aimed at the properties of the weld metal so the joint geometry (Fig. 1b) complied with the ISO2560 standard, designed to avoid dilution with the base plate. Approximately 30 runs were needed to fill the weld gap, with 2–4 beads per layer, deposited at 174 ± 1 A and 25 ± 1 V D.C., with an electrical energy input of $1.08 \pm 0.05\,\mathrm{kJ\,mm^{-1}}$ using an interpass temperature of 250 °C.

The chemical compositions of the welds are given in Table 1; the nitrogen and oxygen concentrations were determined using Leco furnaces whereas the other elements were characterised using spark emission spectroscopy. Note particularly that the carbon concentration is relatively large, and that molybdenum has been added in order to control potential prior–austenite grain boundary embrittlement due to phosphorus; silicon is known to enhance the detrimental effect of phosphorus [26]. The silicon concentration is significantly different for the three welds. The oxygen concentration decreased a little as the silicon concentration was increased; silicon is a known deoxidiser. The other alloying elements are added to control the hardenability as discussed in the next section. [27].

Weld	C	Mn	Si	P	S	Cr	Ni	Mo
A	0.100	2.24	**0.86**	0.009	0.011	0.03	2.11	0.21
B	0.120	2.30	**1.38**	0.009	0.011	0.03	2.12	0.21
C	0.102	2.18	**1.63**	0.009	0.005	0.02	2.07	0.23
Weld	V	Cu	Ti	Sn	As	B	O	N
A	0.017	–	0.024	0.011	0.005	–	**0.0249**	0.0108
B	0.017	–	0.033	0.01	0.005	–	**0.0261**	0.0121
C	0.019	0.03	0.039	0.010	0.013	–	**0.0205**	0.0113

Table 1: Weld–metal chemical compositions, wt%

Transmission electron microscopy was conducted on 3 mm diameter rods machined from the centre of weld C along the welding direction. The specimen preparation technique has been reported elsewhere [28]. The details of the standard mechanical property tests are also described there [28].

3. Microstructure

The main focus of the microstructural work was on the high–silicon weld C. The weld was characterised using optical microscopy, which revealed a rather uniform microstructure not containing allotriomorphic ferrite (α) or Widmanstätten ferrite (α_W), Fig. 2a. The absence of these phases, which are common in low–alloys steel welds, is due to the relatively high hardenability resulting primarily from the combination of carbon, manganese and nickel. This was established by calculation [29] during the design stage of the alloy; some illustrative results are presented in Table 2, where the top row represents the composition of weld C (the concentrations of all other elements are as in in Table 1). Note that changes in the silicon concentration are not expected to significantly influence hardenability [29] so the results in Table 2 apply to all the welds A, B and C.

C	Mn	Ni	V_α	$V_{\alpha W}$
0.10	2.18	2.07	0.00	0.00
0.10	**1.00**	2.07	0.18	0.04
0.10	**1.00**	**1.00**	0.27	0.07
0.05	**1.00**	**1.00**	0.46	0.23

Table 2: Calculated phase fractions of α and α_W as a function of the concentrations of carbon, manganese and nickel in weld C.

Scanning electron microscopy revealed a bit more detail, the microstructure consisting of obvious regions of bainite and martensite (Fig. 2b).

However, both bainite and martensite require transmission electron microscopy to resolve whether the desired microstructure is in fact obtained. Fig. 3 shows that upper bainite has been obtained but with retained austenite films between the fine plates of bainite, instead of the cementite that forms in low–silicon steels. Extensive microscopy failed to reveal any carbides, as might be expected given the large silicon concentration. This also indicates that the material is resistant to tempering since the studies are based on multipass welds where underlying beads are expected to be heat treated on each occasion that new weld metal is deposited. It is worth noting that the scale of the microstructure is consistent with upper bainite, the platelets being submicrometer in thickness [17].

The carbon that is rejected by the bainitic ferrite partitions into the residual austenite, which becomes

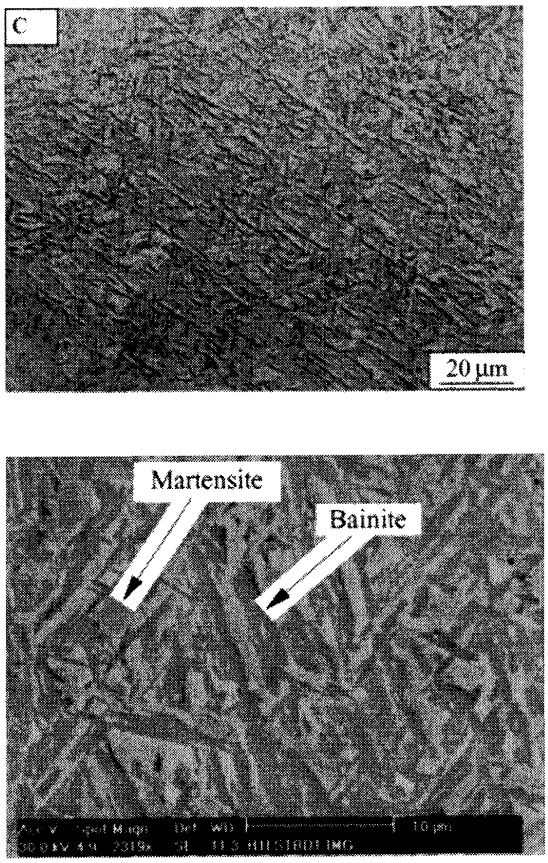

Fig. 2: Weld C: (a) Optical micrograph. (b) SEM micrograph.

enriched with carbon to a concentration approximated by the T_0 curve of the phase diagram [17]. However, it is well known that the carbon is not distributed homogeneously in the remaining austenite. Larger regions of austenite tend to have a lower carbon concentration [30,31,32,17]. It is inevitable that some of the larger regions must decompose by transformation into high–carbon martensite, as illustrated in Fig. 4. Such martensite is probably detrimental to toughness.

4. Mechanical Properties

All–weld metal tensile test results are presented in Fig. 5. There is not much of a variation in strength as a function of the silicon concentration. The proof stress to ultimate tensile strength ratio increases from 0.88 to 0.92 as the silicon concentration changes from about 0.8 to 1.6 wt%. The elongation was in the range 20–23% and the reduction of area in the range 60–62%.

The tensile test data show that in the context of welding alloys, a very high strength has been achieved, in all cases in excess of 830 MPa proof and 950 MPa ul-

Fig. 3: Transmission electron micrograph and corresponding diffraction pattern.

timate strength. This is much higher than in conventional high–silicon welds of the type reported by Evans [25].

Even though the tensile properties are not greatly affected, the toughness improves as the silicon concentration is reduced (Fig. 6). It is speculated that this is because of the effect of silicon in retarding the tempering of martensite. At low silicon concentrations the high–carbon martensite that forms from the enriched–austenite can become tempered during multipass welding, resulting in an improvement in toughness. The silicon is added primarily for the purpose of stopping carbide precipitation but the toughness data show that it is useful to minimise its concentration, but not so much that cementite is induced in the upper bainite microstructure. There is a need for theory capable of optimising the silicon concentration. The remainder of this paper deals with a theory for the effect of silicon on the precipitation of cementite from austenite.

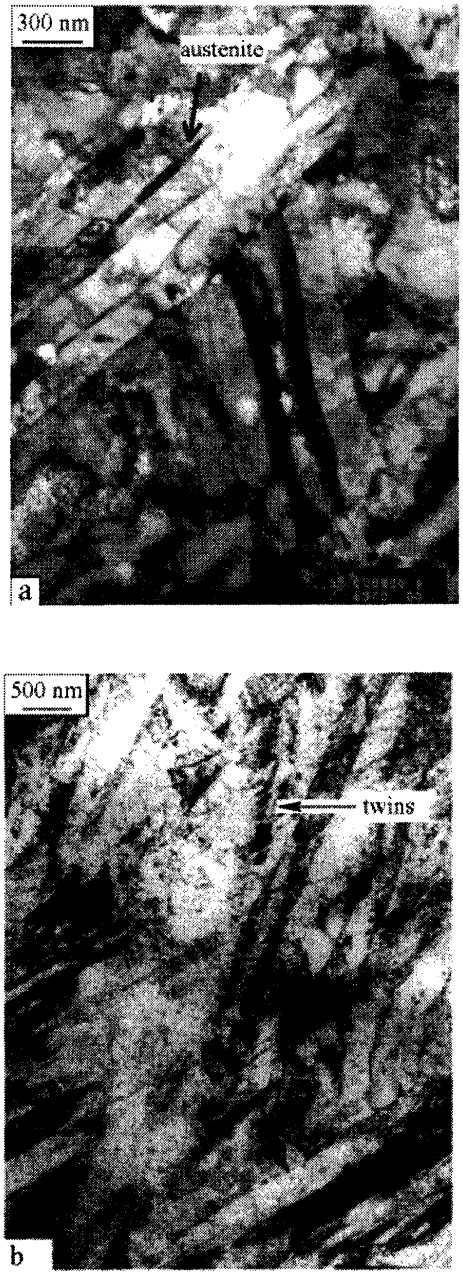

Fig. 4: Transmission electron micrographs of weld C. (a) Shows the expected mixture of bainitic ferrite plates interspersed with retained austenite films. (b) Region containing high–carbon, untempered martensite.

5. Mechanism of Cementite Precipitation

There is good evidence to suggest that the carbides which precipitate from austenite during the formation of upper bainite, grow without the partitioning of substitutional solutes [17]. The mechanism of growth is displacive but the interstitial carbon atoms are mobile so growth occurs at a rate controlled by the diffusion

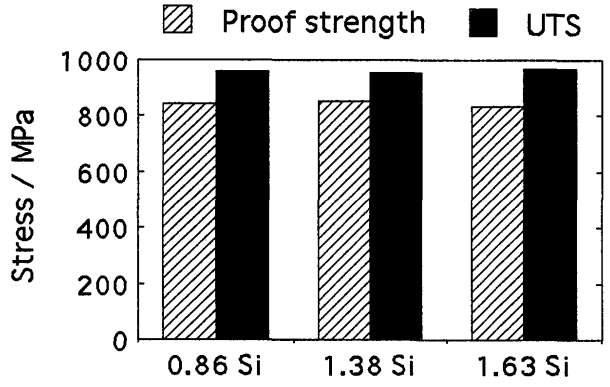

Fig. 6: 0.2% proof stress and ultimate tensile strength data.

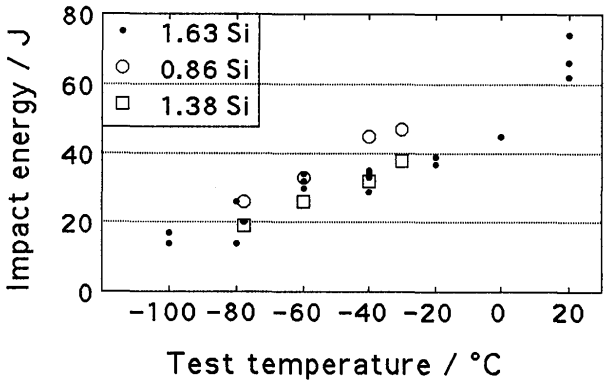

Fig. 6: Charpy impact energies as a function of the test temperature.

of carbon in the austenite ahead of the transformation interface. There exists a constrained equilibrium at the interface, known as *paraequilibrium* [33,34,35], in which the substitutional solutes are configurationally frozen whilst the carbon achieves a uniform chemical potential. This means that the substitutional solute to iron atom ratio remains unchanged on transformation.

Silicon has an incredibly low solubility in cementite. Nevertheless, the displacive mechanism of cementite growth ensures that it becomes trapped in the cementite lattice (paraequilibrium transformation). This reduces the free energy change accompanying the reaction and hence retards precipitation. Given that equilibrium partitioning of silicon is not possible at the temperatures where the cementite associated with upper bainite forms, it is possible that there is no driving force for the paraequilibrium precipitation of cementite, in which case it is completely eliminated, not just retarded.

This hypothesis can be investigated by calculating the equilibrium and corresponding paraequilibrium phase diagrams when austenite (γ) and cementite (θ) coexist.

The calculations are illustrated in Fig. 7, whence it becomes clear that the single–phase austenite field is greatly expanded when transformation is constrained to occur by paraequilibrium mechanism. Notice that for 773 K, the alloy marked **X** falls in the $\gamma + \theta$ field in the equilibrium phase diagram, whereas it falls in the single–phase γ field in the diagram representing paraequilibrium. Since the cementite associated with bainite is constrained to grow by paraequilibrium, it would not in this case precipitate at all.

The phase diagrams illustrated in Fig. 7 have been calculated using MTDATA, which is a Gibbs free energy minimisation algorithm developed by the National Physical Laboratory, U.K. The algorithm is used in conjunction with a thermodynamic database. However, there are no data on the equilibrium composition of cementite in Fe–Si–C systems since the solubility of silicon in cementite is negligible. As a result, this solubility was assumed arbitrarily to be 1 p.p.m. at 298 K and other thermodynamic interactions were assumed to be ideal. This allowed the calculation of both the equilibrium and paraequilibrium phase fields. The assumptions are probably reasonable but cannot strictly be justified so the diagrams are simply there to illustrate a point rather than to make actual predictions. A quantitative treatment of the silicon effect must await progress in the thermodynamic database.

6. Conclusions

By analogy with previous work on wrought steels, it has been possible to design strong weld deposits based on a mixed microstructure of bainitic ferrite, retained austenite and martensite. The resulting welds have good mechanical properties including high strength and reasonable toughness. It is possible that further improvements can be achieved by a better understanding of the role of silicon in the precipitation of cementite from carbon–enriched austenite.

7. Acknowledgments

We congratulate The Joining and Welding Research Institute on its 30th anniversary and for generously supporting the presentation of this paper. We are also grateful to Hugh Davies of the NPL for his support of MTDATA.

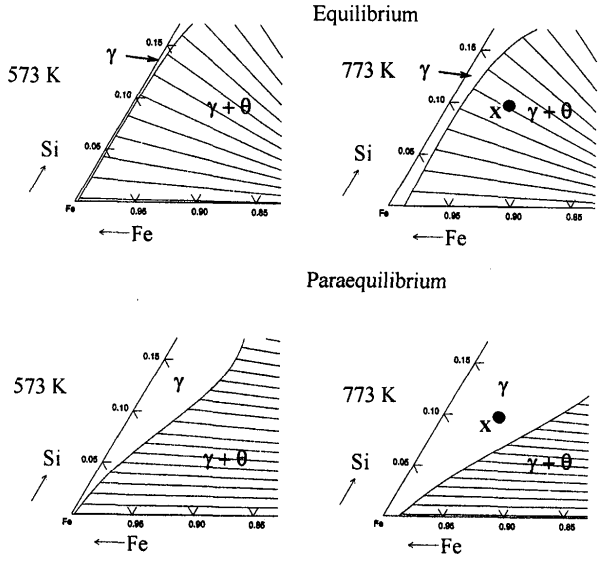

Fig. 7: Calculated equilibrium and corresponding paraequilibrium phase diagrams for the Fe–Si–C system. The concentrations are in mole fractions.

8. References

1. E. C. Bain: *Alloying Elements in Steel,* A. S. M., Cleveland, Ohio, U. S. A. (1939)
2. A. G. Allten and P. Payson: *Trans. ASM* **45** (1953) 498.
3. W. S. Owen: *Trans. ASM* **46** (1954) 812.
4. A. S. Keh & W. C. Leslie: *Materials Sci. Res.* Plenum Press, New York **1** (1963) 208.
5. J. Gordine and I. Codd: *JISI* **207** (1969) 461.
6. R. M. Hobbs, G. W. Lorimer and N. Ridley: *JISI* **210** (1972) 757.
7. F. B. Pickering: *Phase Transformations,* Inst. of Metall., London **2** (1979) VI 7.
8. S. J. Matas and R. F. Hehemann: *Trans. Metall. Soc. A. I. M. E.* **221** (1961) 179.
9. R. Entin: *Decomposition of Austenite by Diffusional Processes,* Intersci, NY (1962) 295.
10. J. Deliry: *Mem. Sci. Rev. Metall.* **62** (1965) 527.
11. J. Pomey: *Mem. Sci. Rev. Metall.* **63** (1966) 507.
12. R. F. Hehemann : *Phase Transformations,* ASM, Metals Park, Ohio (1970) 397.
13. R. Le Houillier, G. Begin and A. Dubé: *Metall. Trans.* **2A** (1971) 2645.
14. H. K. D. H. Bhadeshia and D. V. Edmonds : *Metall. Trans.* **10A** (1979) 895.
15. B. P. J. Sandvik: *Metall. Trans. A* **13** (1982) 777.
16. B. P. J. Sandvik: *Metall. Trans. A* **13** (1982) 789.
17. H. K. D. H. Bhadeshia: *Bainite in Steels,* Institute of Materials, London (1992) 1–458.
18. H. K. D. H. Bhadeshia and D. V. Edmonds: *Metal Science* **17** (1983) 411.
19. H. K. D. H. Bhadeshia and D. V. Edmonds: *Metal Science* **17** (1983) 421.
20. V. T. T. Miihkinen and D. V. Edmonds: *Materials Science and Technology* **3** (1987) 422.
21. H. K. D. H. Bhadeshia: *Encyclopaedia of Materials: Science and Technology,* Elsevier Science Ltd. (2002) 1.
22. F. G. Caballero, H. K. D. H. Bhadeshia, K. J. A. Mawella, D. G. Jones and P. Brown: *Materials Science and Technology* **17** (2001) 512.
23. F. G. Caballero, H. K. D. H. Bhadeshia, K. J. A. Mawella, D. G. Jones and P. Brown: *Materials Science and Technology* **17** (2001) 517.
24. F. G. Caballero, H. K. D. H. Bhadeshia, K. J. A. Mawella, D. G. Jones and P. Brown: *Materials Science and Technology* **18** (2002) 279.
25. G. M. Evans: *Metal Construction* **18** (1986) 438R.
26. C. J. McMahon Jr.: *Innovations in Ultrahigh-Strength Steel Technology,* eds G. B. Olson, M. Azrin and E. S. Wright, Sagamore Army Res. Conf. USA (1987) 597.
27. H. K. D. H. Bhadeshia and L.–E. Svensson: *Mathematical Modelling of Weld Phenomena,* Institute of Materials, London, eds H. Cerjak and K. E. Easterling (1993) 109.
28. M. Lord: *Ph.D. Thesis,* University of Cambridge (1999)
29. H.K.D.H. Bhadeshia, L.–E. Svensson and B. Gretoft: *Acta Metallurgica* **33** (1985) 1271.
30. A. Schrader and F. Wever: *Arch. Eisenhuttenwesen* **23** (1952) 489.
31. S. J. Matas and R. F. Hehemann: *Trans. Metall. Soc. AIME* **221** (1961) 179.
32. H. K. D. H. Bhadeshia & A. R. Waugh: *Acta Metall.* **30** (1982) 775.
33. A. Hultgren: *Jernkontorets Ann.* **135** (1951) 403.
34. M. Hillert: *Report,* Swedish Inst. for Metals Research, Sweden (1953)
35. H. K. D. H. Bhadeshia: *Progress in Materials Science* **29** (1985) 321.